Available online at www.sciencedirect.com
SCIENCE DIRECT®
Bioorganic & Medicinal Chemistry 13 (2005) 6070–6082
Bioorganic & Medicinal Chemistry

DFT-based ranking of zinc-binding groups in histone deacetylase inhibitors

K. Vanommeslaeghe,[a,b,*] S. Loverix,[b,c] P. Geerlings[b] and D. Tourwé[a]

[a]*Vrije Universiteit Brussel, Organic Chemistry Group, Pleinlaan 2, B-1050 Brussel, Belgium*
[b]*Vrije Universiteit Brussel, General Chemistry Group, Pleinlaan 2, B-1050 Brussel, Belgium*
[c]*Vlaams Interuniversitair Instituut voor Biotechnologie, Department of Molecular and Cellular Interactions, Pleinlaan 2, B-1050 Brussel, Belgium*

Received 2 April 2005; revised 2 June 2005; accepted 3 June 2005
Available online 11 July 2005

Abstract—Histone deacetylases (HDACs) have recently attracted considerable interest as targets in the treatment of cell proliferative diseases such as cancer. In the present work, a general framework is proposed for chemical groups that bind into the HDAC catalytic core. Based on this framework, a series of groups was selected for further investigation. A method was developed to rank the HDAC inhibitory potential of these moieties at the B3LYP/6-31G* level, making use of extra diffuse functions and of the PCM solvation model where appropriate. The resulting binding geometries indicate that very stringent constraints should be satisfied in order to have bidental zinc chelation, and even more so to have a strong binding affinity, which makes it difficult to predict the binding mode and affinity of such zinc-binding groups. The chemical hardness and the pK_a were identified as important criteria for the binding affinity. Also, the hydrophilicity may have a direct influence on the binding affinity. The calculated binding energies were qualitatively validated with experimental results from the literature, and were shown to be meaningful for the purpose of ranking. Additionally, the insights gained from the present work may be useful for increasing the accuracy of QSAR models by providing a rational basis for selecting descriptors.

1. Introduction

Histone deacetylases (HDACs) are very promising targets for so-called mechanism-based anticancer drugs, which may combine clinical efficacy with relatively mild toxicological side-effects.[1,2] Medicinal applications of HDAC inhibitors are however not limited to the treatment of cancer, but may vary from fibrotic diseases,[3] including liver fibrosis,[4,5] an important cause of death in Western society, over autoimmune[6] and inflammatory[7] diseases, to polyglutamin disease.[8,9] Also, they have been shown to inhibit dedifferentiation in cell cultures.[5] Not only do HDACs regulate chromatin structure, recent discoveries indicate that the HDAC isoform HDAC6 actually functions as a tubulin deacetylase and plays a major role in tubulin remodelling events, which are vital for mitosis.[10]

TSA (Trichostatin A, **1**) was the first potent HDAC inhibitor discovered.[11] Although the synthesis[12] of the compound itself is too complex to allow economical pharmaceutical use and its metabolisation is too rapid,[13] it was an interesting lead compound for the development of HDAC inhibitors as it features a high affinity for HDAC[14] and a small size in comparison with other natural HDAC inhibitors like Trapoxin B[15] (**2**). Following the discovery of the HDAC inhibitory activity of the antitumour agent TSA,[11] a wide variety of HDAC inhibitors has been identified, synthesised and tested.[16] Some of these products are already in clinical trials,[17] such as MS-275[18] (**3**), which is in phase II, and SAHA[19] (suberoylanilide hydroxamic acid, **4**), which has recently entered phase III (Fig. 1).

As can be seen in X-ray structures of inhibitor-bound HDLP,[20] an HDAC analogue with the same active site as any member of the HDAC family, and of HDAC8,[21,22] an HDAC isoform, the active site consists of a narrow apolar pocket, at the bottom of which the polar catalytic core can be found, containing a zinc ion. This geometry is reflected in the common template

Keywords: Histone deacetylase inhibition; Density functional theory; Quantitative structure–activity relationships; Zinc hydrolase.
* Corresponding author. Tel.: +32 2 6293300; fax: +32 2 6293304; e-mail: Kenno.Vanommeslaeghe@vub.ac.be

0968-0896/$ - see front matter © 2005 Elsevier Ltd. All rights reserved.
doi:10.1016/j.bmc.2005.06.009

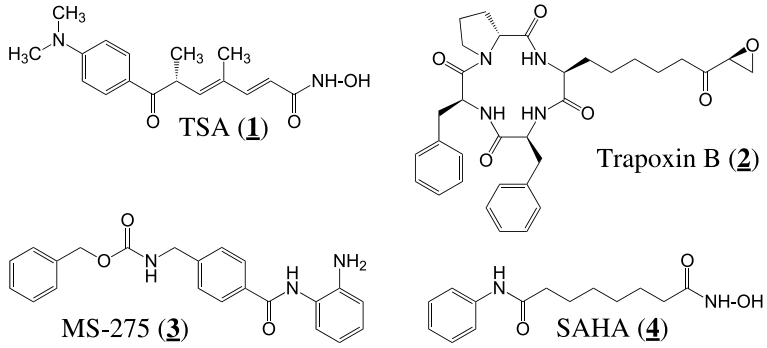

Figure 1. Molecular structures of TSA (**1**), Trapoxin B (**2**), MS-275 (**3**) and SAHA (**4**).

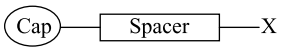

Figure 2. Common template for HDAC inhibitors. 'Cap', cap group that binds on the surface of the protein and supposedly is responsible for specificity. 'X', zinc-binding, enzyme-inhibiting group. 'Spacer', links the cap and X groups and must fit into the narrow hydrophobic pocket.

for HDAC inhibitors, which was proposed by Jung et al.[23] before any of the above-mentioned X-ray structures were available (Fig. 2).

Extensive research has been conducted on the derivatisation of the cap group and the spacer, yielding potent[24–26] and in some cases isoform-selective[27,28] HDAC inhibitors.[29] Also, efforts have been made to model the binding of HDAC inhibitors using empirical methods.[14,30–32] However, most of these computational and synthetic studies were focused on hydroxamate-based inhibitors. Although the hydroxamate moiety is known to strongly bind to the HDAC catalytic core, it is pharmacokinetically unfavourable.[13,33] However, combinatorial studies on the zinc-binding moiety proved it difficult to find other potent HDAC-inhibiting groups.[34–36] Noteworthy exceptions are the thiol group and the mercaptoacetamide group, on the basis of which fairly potent inhibitors were recently described,[37,38] and the *o*-aminoanilide group,[39] which features as a zinc chelator in MS-275 (**3**). These examples prove that alternative zinc ligands may be of interest. Still, we feel that a large part of the possible chemical space of the zinc-binding group is still unexplored. Therefore, we evaluate some alternatives with theoretical calculations, in order to provide guidelines for the selection of new synthetic targets.

2. Methodology

Previously, we conducted an extensive study of the HDAC active site,[40,41] using models based on the X-ray structure of HDLP,[20] which was the only available structure that provided information in this respect. After completion of the present work, X-ray structures of inhibitor-bound human HDAC8, were published by two independent groups,[21,22] showing that the catalytic core geometry is essentially the same as in HDLP,[41] which confirms the validity of our model for the HDAC

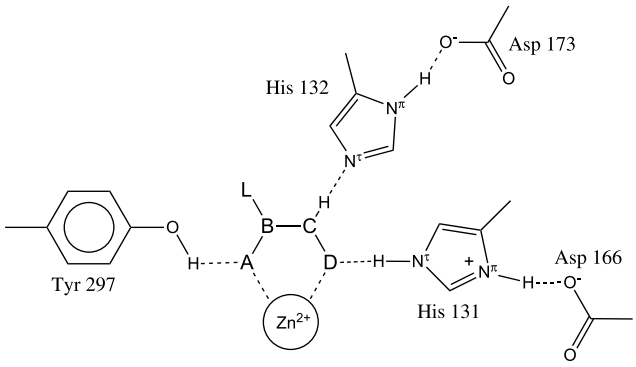

Figure 3. Common framework for bidentate zinc chelators as HDAC inhibitors.

active site. The catalytic core comprises a Zn^{2+} ion coordinated by two histidine residues and an aspartate, two His–Asp dyads and a tyrosine residue. This structural motif forms the polar bottom of the apolar active site pocket, and is the target of the present study. From previous work, a general framework for the catalytic core-binding moiety can be derived (Fig. 3)[†] where

- A should be a soft nonbonding electron pair donor in order to coordinate the zinc ion[42] and a H-bond acceptor in order to accept a hydrogen bond from the tyrosine OH. A H-bond donor may also be valid because in that case, a H-bond could be donated to the phenolic oxygen of Tyr 297.
- B should link the zinc-chelating moiety to the spacer and hence be at least trivalent.
- C should be a H-bond donor in order to donate a H-bond to His 132. Consequently, C also needs to be trivalent or higher.
- D should be a proton donor, in order to protonate His 131 and subsequently accept an ionic H-bond from it and form a strong interaction with the zinc ion.
- L links the zinc-chelator to the spacer.

Considering this framework, it can be easily seen why hydroxamates are such good HDAC inhibitors. However, for therapeutic purposes, these compounds

[†] Throughout this article, the residue numbering from HDLP will be used.

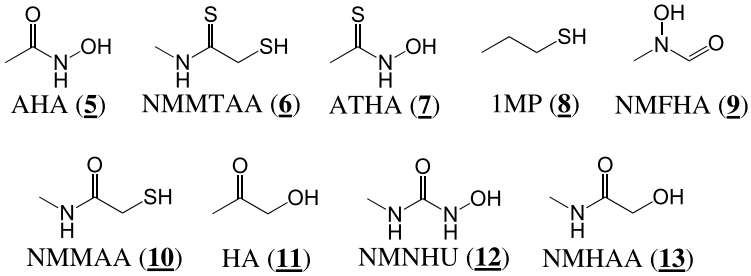

Figure 4. Molecular fragments studied in the present work. **5**, acetohydroxamic acid (AHA); **6**, *N*-methyl-mercaptothioacetamide (NMMTAA); **7**, acetothiohydroxamic acid (ATHA); **8**, 1-mercaptopropane (1MP); **9**, *N*-methyl-formohydroxamic acid (NMFHA); **10**, *N*-methyl-mercaptoacetamide (NMMAA); **11**, hydroxyacetone (HA); **12**, *N*-methyl-*N*′-hydroxyurea (NMNHU); **13**, *N*-methyl-hydroxyacetamide (NMHAA).

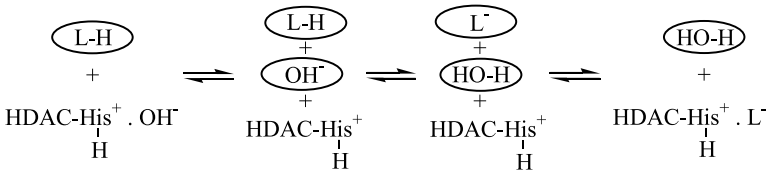

Scheme 1. Formal mechanism for calculating the binding energy of an inhibitor L, relative to a hydroxide ion. The ovals denote an aqueous environment.

often suffer considerable drawbacks and as a consequence, alternative chemical moieties fitting this framework are sought. On the basis of the framework in Figure 3, similarity to known inhibitors of other zinc hydrolases, and synthetic feasibility, nine groups were selected for in silico testing (Fig. 4).

Because metal coordination in general and zinc coordination in particular remains a problem for classical scoring functions and force fields,[43,44] ranking a dataset of zinc ligands with such methods would be inadequate. Therefore, the scoring in this study will be based on the quantum chemically determined energy of interaction between the proposed ligand and the active site. More specifically, a DFT method was chosen because this allows for inclusion of electron-correlation effects, necessary for accurate determination of intermolecular interactions, at a relatively modest computational cost.

Apart from the interaction energy between the active site and the ligand, solvation and protonation effects also influence the energy of interaction. The solvation can be included at an acceptable computational cost by employing a continuous solvent model for the calculations on the free ligand. No solvent model was used for the calculations on the catalytic core because it is buried at the bottom of a narrow hydrophobic pocket. As for the protonation, a previous study showed that a water molecule in the HDAC active site is spontaneously deprotonated by His 131, partially because of the acidifying effect of the zinc coordination.[41] Thus, it can be argued that any zinc-binding group with an estimated pK_a lower than that of water also binds as an anion. This is probably the case for all of our proposed molecular fragments. Nevertheless, as these are weak to very weak acids, in solution, they will be present almost exclusively in protonated form. Consequently, the proton affinity of the ligand has to be subtracted from the binding energy. However, on binding, the ligand displaces the above-mentioned hydroxide-ion from the active site, which will in turn be protonated in solution, counteracting the contribution of the ligand's proton affinity to the energy. Overall, the process depicted in Scheme 1 has to be considered. The energy associated with this process is given by Eq. 1. In the present study, this energy will be determined for the set of possible ligands presented above, as a measure of their HDAC inhibitory potential.

$$\begin{aligned}\Delta E_{\text{tot}} = &-\Delta E(\mathrm{E^+OH^-}) + [E'^{\mathrm{OH^-}}_{\mathrm{HOH}}(\mathrm{OH^-}) \\ &- E^{\mathrm{OH^-}}_{\mathrm{bind(EOH)}}(\mathrm{OH^-})] + \Delta E'(\mathrm{H^+OH^-}) \\ &+ [E^{\mathrm{E^+}}_{\mathrm{bind(EL)}}(\mathrm{E^+}) - E^{\mathrm{E^+}}_{\mathrm{bind(EOH)}}(\mathrm{E^+})] \\ &- \Delta E'(\mathrm{H^+L^-}) - [E'^{\mathrm{L^-}}_{\mathrm{HL}}(\mathrm{L^-}) - E^{\mathrm{L^-}}_{\mathrm{bind(EL)}}(\mathrm{L^-})] \\ &+ \Delta E(\mathrm{E^+L^-})\end{aligned} \quad (1)$$

This equation describes the method for calculating the total binding energy ΔE_{tot}[§] of a ligand in the active site of HDAC. $E^{\mathrm{C}}_{\mathrm{B}}(\mathrm{A})$ denotes the energy of molecule A at geometry B and with the basis sets of C, A and C being either the enzyme E, the ligand L or the complex EL. $\Delta E(\mathrm{AC})$ denotes the interaction energy between A and C. E' denotes the energy calculated using a solvent model, as opposed to the vacuum energy E.

3. Computational details

3.1. Catalytic core model

To the HDLP/TSA complex obtained from the Brookhaven Protein Data Bank[45] (entry code 1C3R, resolu-

§ Strictly spoken, a double delta (in this case $\Delta\Delta E_{\text{tot}}$) should be written, but in order not to complicate notation, single deltas will be used throughout this article.

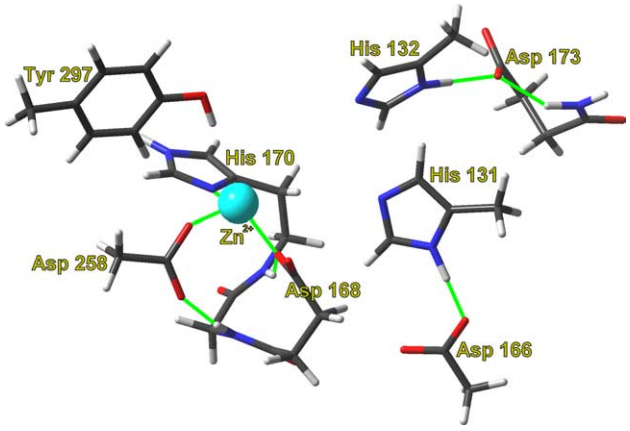

Figure 5. Empty catalytic core model for HDAC.

tion: 2.1 Å), hydrogen atoms were added, and their positions were optimised using the ESFF force field[46] as implemented in the Insight II software.[47] The resulting geometry was used as a starting point for the generation of the catalytic core model containing a total number of 103 atoms, shown in Figure 5.

This model comprises the catalytically important zinc ion, together with the side chains of its coordinating residues Asp 168, His 170 and Asp 258. The main chain between Asp 168 and His 170 was retained, because the hydrogen bonds from aspartates 168 and 258 to the two amide NH atoms in this backbone segment will likely influence the electrostatic interactions upon coordination of the catalytic zinc ion. The phenolic side chain of Tyr 297 was included, as well as the side chains of the two His–Asp pairs, His 131–Asp 166 and His 132–Asp 173, because of their role in binding and catalysis.[20–22] Finally, the C_α atom of Asp 173 was retained, together with the carbonyl group of Asp 173 and the NH group of Gly 174, because this NH is hydrogen bonded to Asp 173, which may directly influence the basicity of the whole dyad. We consider this model sufficiently extended for a pure quantum chemical approach, as the closest polar centre that was not included in the model is the amide nitrogen of Gly 295, located at a distance of 4.6 Å from the catalytic Zn^{2+} ion, and the closest charged group is a sodium ion at 7.4 Å.[¶] Moreover, these groups, as well as all other polar moieties surrounding the catalytic side model, are shielded from the catalytic Zn^{2+} ion by bulk protein, so that they are not likely to interfere directly with inhibitor binding. On this model system, a DFT/B3LYP study was conducted, using the 6-31G* basis set as a starting point for all atoms. Diffuse functions were added to all nonhydrogen atoms involved in binding or in proton transfers (the catalytic zinc ion, the phenolic oxygen atom of Tyr 297, the four nitrogen atoms of His 131 and His 132 and the four side chain oxygen atoms of Asp 166 and Asp 173) and to any nitrogen, oxygen and sulfur atoms present in the ligand. Throughout this work, Gaussian 03[48] was used for all subsequent DFT calculations, using the default convergence criteria for the energy minimisations and "tight" convergence criteria for any SCF calculations.

[¶] Vannini et al. argue that this Na^+ ion may need to be replaced by a K^+ ion in order for HDAC8 to display optimal stability and catalysis.[22]

3.2. Full minimisation of catalytic core model

Prior to evaluating the interactions of this model with different ligands, a full minimisation was attempted in the presence of hydroxamate AHA (**6**), the common zinc-chelating group of all HDAC inhibitors used in crystallographic studies.[20–22] Only the atoms in our model that were originally connected to the rest of the protein were frozen, namely the C_α atoms of Asp 168, His 170 and Asp 173, the backbone N atom of Gly 174, and the C_β atoms of His 131, His 132, Asp 166, Asp 258 and Tyr 297. This minimisation took a considerable amount of computer time, and more importantly, unlikely geometrical deviations were observed in the final structure. For these reasons, a more rigid approach was adopted for the evaluation of the protein–ligand interactions.

3.3. Protein–ligand interaction

The original catalytic core model described above was again taken as a starting point. Based on the binding geometry of the hydroxamate moiety of TSA in HDLP, molecular fragments were manually docked into this model. Subsequently, energy minimisations were performed, this time keeping the heavy atoms of the X-ray structure fixed. The whole ligand was allowed to move, as well as all of the hydrogen atoms present in the active site. In the case of AHA, this approach took about half the CPU time of the above-mentioned full minimisation. After the optimisations reached convergence, protein–ligand interaction energies were calculated using the counterpoise method for correcting the Basis Set Superposition Error (BSSE).[49]

3.4. Aqueous deprotonation of the ligand

Prior to the determination of a ligand's proton affinity, its respective solution conformation needs to be established. Because a full conformational analysis at B3LYP/6-31G* level including a solvent model would computationally be rather costly, for each ligand, a systematic conformational search was set up at HF/3-21G* level in vacuum, using Spartan 5.1.[50] The resulting minima within an energy window of 10 kcal mol^{-1} above the absolute minimum and differing more than 0.2 Å rms after superposition were then further refined at B3LYP/6-31G* level with Gaussian 03, adding diffuse functions on all noncarbon, nonhydrogen atoms and using the PCM[51–53] solvent model. Finally, the minimum with the lowest solvated energy was selected for determining its proton affinity. PCM proton affinities were not BSSE corrected because this method for constructing the solvent cavity is incompatible with the counterpoise correction scheme.

3.5. Chemical hardness of the ligand

Similar to the determination of the proton affinity, the chemical hardness was calculated for each ligand. First,

the selected minima from the HF/3-21G* searches were refined at B3LYP/6-31G* level in vacuum, with the inclusion of the same diffuse functions as described above. Then, the vertical ionisation energy (I) and electron affinity (A) of the lowest minimum was determined by calculating the energy of its doublet state anion and cation. This makes it possible to estimate the global hardness of the ligand, using the finite difference approach: $\eta = (1/2)(I - A)$. However, since the molecules considered here are all closed-shell structures, the values for A are always negative. In this case, the applicability of the above-mentioned formula is debatable, and A is set equal to zero, so that the chemical hardness is reduced to $\eta = (1/2) I$.[54]

4. Results and discussion

4.1. Binding geometries

After the minimisations of the different ligands in the active site, the fixed atoms in the final geometries of all of the ligands were superposed, as depicted in Figure 6. Additionally, some relevant noncovalent bond distances are listed in Table 1. Hydrogen bonds are identified by the following geometric criterion: the H···A distance d should be smaller than 2.7 Å, and the D–H···A angle θ should be larger than 90°.[55] In case the acceptor is a sulfur atom, the maximum distance was increased to 3.0 Å, in order to compensate for the fact that sulfur's van der Waals' radius is 0.3 Å larger than oxygen's. However, this criterion is designed to include even the weakest hydrogen bonds. In our dataset, there is a clear segregation into moderate hydrogen bonds (d = 1.6–2.2 Å, or 2.2–2.4 Å in case the acceptor is sulfur, and $\theta > 120$ °, marked green in the table) and weak hydrogen bonds (d = 2.5–2.7 Å, or 2.9 Å in case the acceptor is sulfur, marked yellow in the table). It should also be noted that the two hydrogen bonds having a carbon atom as a donor that fall into the range of the moderate hydrogen bonds (coloured blue in Table 1), are expected to be roughly half as strong as the other members of this group.[56,57]

Despite the use of a bidentate template for the choice of the ligands, many of the optimised structures coordinate the catalytic zinc ion in a monodentate fashion, resulting in a nearly perfect tetrahedral coordination (Figs. 6B and C). In fact, next to AHA (**5**), which is a known bidentate chelator in this context,[20–22,40] only NMFHA (**9**) and NMNHU (**12**) bind in a bidentate fashion. These two zinc-chelating groups are chemically very similar to the hydroxamate (**5**), and display a binding mode that is almost identical to AHA's (**5**) (Fig. 6A), and very similar to the binding mode of the hydroxamate function in the available inhibitor-bound X-ray structures.[20–22] The monodentate binding mode of the other molecular fragments may be attributed to a combination of the following factors:

- an unfavourable geometry of the proposed zinc-binding centres A and D,
- a favourable interaction between the ligand and His 170,
- a hydrogen bond between L and His 132.

This is supported by the fact that, surprisingly, monodentate coordination occurs for all sulfur-containing groups, and the atom that coordinates the zinc is always atom D, whether this is the sulfur atom or, in the case of **7**, an oxygen atom. Since sulfur is thought to interact well with zinc,[37,38,42,58] the monodentate binding mode of ATHA (**7**) indeed suggests that the inhibitor-exposed surface area of the catalytic zinc ion is simply too small to accommodate both the relatively large sulfur atom and a second coordinating centre.

Still, these arguments do not explain why HA (**11**) and NMHAA (**13**) also bind in a monodentate fashion. This could be attributed to the presence of an sp^3 carbon at position C, which might give rise to a geometric preference that disfavours bidentate chelation. Indeed, all molecules in which this is the case, bind in a monodentate fashion. However, within our dataset, the difference in distance between the two zinc-coordinating oxygen atoms is 0.05 Å at most, so it is very unlikely that this geometrical factor has a significant impact on the binding mode. Rather, the hydrogen bond between atom C and His 132 might be required to force the ligand into bidentate chelation. This, in turn, suggests that the electronegative sp^2 carbon atom in NMFHA (**9**) is a sufficiently strong hydrogen bond donor to influence the binding geometry. It also implies that, in this specific environment, a tetrahedral zinc coordination might be preferred over the 'distorted tetragonal pyramid' geometry that is observed when a five-membered chelate ring is formed by binding an appropriate bidentate chelator in the active site. This should not necessarily be disadvantageous for the catalytic activity, since in the tetrahedral transition state of the proposed catalytic mechanism, a four-membered chelate ring is formed.

One noteworthy exception in our dataset is NMMTAA (**6**). As already suggested by the conformational searches preceding the determination of the proton affinity (see Section 3), the size of the two sulfur atoms excludes any gauche conformations, resulting in a trans conformation, which prohibits bidentate chelation and causes a totally different binding mode. However, this does not explain the monodentate coordination for the other sulfur-containing zinc-binding groups, as it does not occur with ATHA (**7**, perfectly cisoid thioamide bond) and NMMAA (**10**, ABCD torsion angle = 27°).

It should also be noted that, when the present binding geometries are transposed into the complete HDLP active site, some steric clashes arise with Phe 198. This residue was not included in our active site model because, if the ligands had bound in a bidentate fashion, it would have been out of their reach. However, after the minimisation, in which a monodentate coordination was adapted, the terminal methyl groups of NMMTAA (**6**) and NMHAA (**13**) occupy the same space as Phe 198. Consequently, the actual binding geometries and energies of these groups may vary significantly from the present result. Although this does not affect our discussion

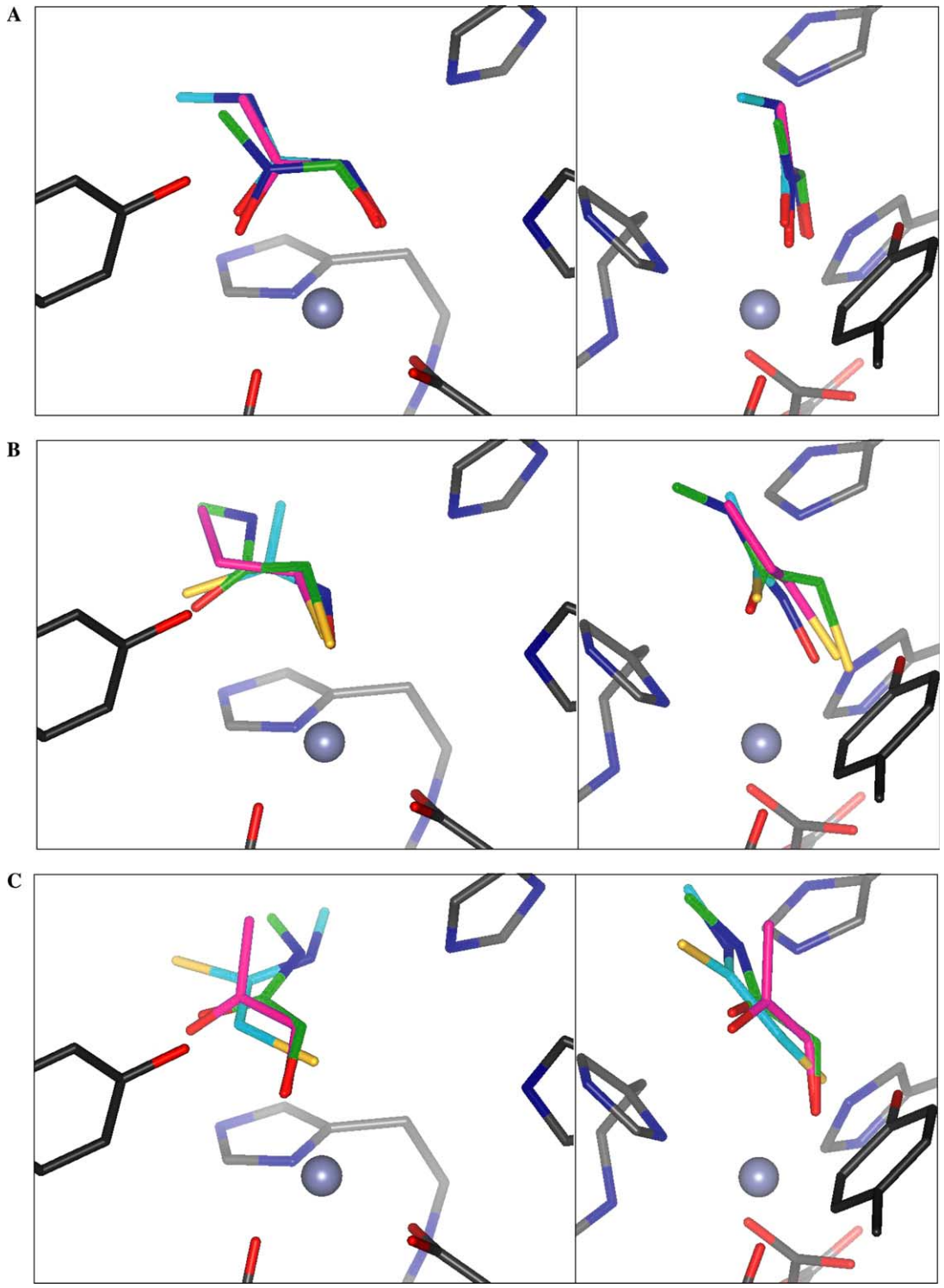

Figure 6. (A) Front and side views of the final conformation of NMFHA (**9**, carbon atoms in green), AHA (**5**, carbon atoms in magenta) and NMNHU (**12**, carbon atoms in cyan) in the catalytic core of HDAC. (B) Front and side views of the final conformation of 1MP (**8**, carbon atoms in magenta), NMMAA (**10**, carbon atoms in green) and ATHA (**7**, carbon atoms in cyan) in the catalytic core of HDAC. (C) Front and side views of the final conformation of HA (**11**, carbon atoms in magenta), NMHAA (**13**, carbon atoms in green) and NMMTAA (**6**, carbon atoms in cyan) in the catalytic core of HDAC. Hydrogen atoms are omitted for the sake of clarity.

regarding the factors that influence binding affinity, no predictions can be made about the actual binding geometry and affinity of these two groups. Likewise, the methyl group of ATHA (**7**) and NMMAA (**10**) makes sterical contact with Phe 198. In these cases, only small deviations from the present geometries are expected.

Table 1. Lengths (Å) of noncovalent bonds between the ligand and the HDAC catalytic core

Compound	A-Zn[a]	A-Y297OH[a]	D-Zn[a]	D-H131N$^{\tau}$H[a]	D-Y297OH[a]	CH-H132N$^{\tau}$H[a]	LH-H132N$^{\tau}$H[a]
AHA (**5**)	2.335	1.642	2.035	1.865	n/a	1.714	n/a
NMNHU (**12**)	2.500	1.656	1.996	1.938	n/a	1.722	n/a
NMFHA (**9**)	2.240	1.602	2.098	1.985	n/a	1.962	n/a
ATHA (**7**)	n/a	2.266	1.979	2.881	2.731	1.906	2.601
NMMAA (**10**)	n/a	2.801	2.292	2.947	2.256	2.143	3.174
1MP (**8**)	n/a	n/a	2.296	3.035	2.254	2.663	n/a
HA (**11**)	n/a	3.104	1.945	3.718	1.813	2.522	n/a
NMHAA (**13**)	n/a	3.251	1.942	3.758	1.772	2.500	2.008
NMMTAA (**6**)	n/a	n/a	2.334	3.201	2.322	n/a	2.006

Moderate hydrogen bonds are marked in green, weak hydrogen bonds in yellow (see text for a discussion of the criterion on which this distinction is based). Bond lengths involving a sulfur atom are coloured red; possible hydrogen bonds with carbon acting as a donor are coloured blue.
[a]see Fig. 3.

Still, the binding energies, which are sensitive to subtle geometric effects, cannot be relied upon for predictive purposes. Also, while the bidentate chelators are expected to have little or no conformational freedom, the same cannot be said for the monodentate ligands. Moreover, some of our monodentate binding groups, in particular the sulfur-containing moieties, may in fact be able to adapt a bidentate binding mode if they are capable of inducing large geometric deviations in the active site, which our model does not allow. By consequence, for all monodentate ligands except 1MP (**8**), there is a reasonable probability that the present geometries differ significantly from the lowest-energy binding modes, and that the actual binding affinities are more favourable than the estimated ones (see below).

4.2. Binding energies

The binding energies of the ligands, as calculated in Eq. 1, are the sum of four contributions:

1. The relative 'vertical' proton affinity of the ligand, defined as the energy of transferring a proton from the ligand to a hydroxide ion in aqueous environment:

$$\Delta E_{\text{prot}} = \Delta E'(\text{H}^+\text{OH}^-) - \Delta E'(\text{H}^+\text{L}^-). \qquad (2)$$

2. The energetic cost of bringing the active site from its hydroxide-bound conformation to its ligand-bound conformation:

$$\Delta E_{\text{conf}} = [E^{\text{E}^+}_{\text{bind(EL)}}(\text{E}^+) - E^{\text{E}^+}_{\text{bind(EOH)}}(\text{E}^+)]. \qquad (3)$$

3. The relative interaction energy of the ligand, defined as the difference in interaction energy between the hydroxide-bound active site and the ligand-bound active site:

$$\Delta E_{\text{inter}} = \Delta E(\text{E}^+\text{L}^-) - \Delta E(\text{E}^+\text{OH}^-). \qquad (4)$$

4. The energy of bringing the deprotonated ligand from its protonated conformation in solution to its binding conformation in vacuum, relative to the hydroxide ion:

$$\Delta E_{\text{residu}} = [E'^{\text{OH}^-}_{\text{HOH}}(\text{OH}^-) - E^{\text{OH}^-}_{\text{bind(EOH)}}(\text{OH}^-)] - [E'^{\text{L}^-}_{\text{HL}}(\text{L}^-) - E^{\text{L}^-}_{\text{bind(EL)}}(\text{L}^-)]. \qquad (5)$$

Physically spoken, this residual term consists of the relaxation energy of the ligand after deprotonation, the desolvation energy of the ligand and the energetic cost of bringing the ligand in its binding conformation, all of this relative to the hydroxide ion. These three contributions cannot be obtained separately without substantial additional calculations. Based on the observation that the absolute $[E'^{\text{L}^-}_{\text{HL}}(\text{L}^-) - E^{\text{L}^-}_{\text{bind(EL)}}(\text{L}^-)]$ values are always above 60 kcal mol^{-1}, which is, especially in the case of the OH$^-$-ion, too large to reflect a purely conformational change, we speculate that the trends in ΔE_{residu} roughly reflect trends in desolvation energies.

These different contributions are listed in Table 2, together with the total binding energies, as well as the chemical hardnesses of the protonated ligands in their respective lowest energy conformation in vacuum.

Two of the three bidentate chelators, AHA (**5**) and NMNHU (**12**), have the most favourable ΔE_{inter}, and as these groups are chemically very similar, their difference in ΔE_{inter} is insignificant. Surprisingly, NMHAA (**13**), a monodentate ligand, also has a similar ΔE_{inter}, while the ΔE_{inter} of NMFHA (**9**), the third bidentate chelator, is 11.4 kcal mol^{-1} less optimal. The former case can be explained by the presence of a hydrogen bond between the amide linker and His 132, while in the latter case, a weak hydrogen bond, in which carbon acts as a donor, is present between centre C and His 132. This indicates that centre C plays an important role in inhibitor binding, confirming similar findings in the discussion of the binding geometries. To further explain the weak ΔE_{inter} of NMFHA (**9**) one should consider that this fragment is the only one in the dataset that lacks a negative charge on centre D, which should form an ionic hydrogen bond with His 131, as in AHA (**5**).

It is also noteworthy that the sulfur-containing ligands (**6**–**8** and **10**) have the least optimal ΔE_{inter}, by a large margin: the difference in ΔE_{inter} between NMMAA (**10**) and NMFHA (**9**) is 7.4 kcal mol^{-1}. One could argue that, in spite of what is commonly stated, sulfur is perhaps not a good zinc-binding centre in this particular case. However, this still does not explain why ATHA (**7**), in which the oxygen atom instead of the sulfur atom

Table 2. Energetic contributions (kcal mol^{-1}), estimated HDAC-binding energies (kcal mol^{-1}) and chemical hardnesses η (kcal mol^{-1}) of molecular fragments 1–10

Compound	ΔE_{prot}	ΔE_{conf}	ΔE_{inter}	ΔE_{residu}	ΔE_{tot}	η
NMMTAA (**6**)	−25.5	−0.3	35.6	−23.5	−13.7	93.8
AHA (**5**)	−13.6	0.6	8.5	−5.8	−10.3	110.7
ATHA (**7**)	−21.9	0.4	29.3	−16.9	−9.2	101.2
1MP (**8**)	−19.2	0.1	30.4	−19.2	−8.0	105.0
NMFHA (**9**)	−14.1	0.3	19.9	−11.6	−5.5	106.2
NMMAA (**10**)	−23.2	−0.1	27.3	−6.9	−2.9	103.9
HA (**11**)	−0.9	−0.5	13.1	−11.3	0.4	117.8
NMNHU (**12**)	−8.5	0.8	8.4	1.7	2.5	109.7
NMHAA (**13**)	−2.8	−1.3	8.5	−0.3	4.0	110.8

coordinates the zinc ion, falls within the range of the sulfur-containing compounds. A more satisfactory explanation is provided by the chemical hardness. As shown in Figure 7, there is a significant correlation between this descriptor and the ΔE_{inter}. The slope of the curve suggests that, contrary to our criteria for selecting candidate zinc-binding groups, harder groups are better ligands, and despite the supposed 'softening' effect of the His–Asp dyads, the catalytic core as a whole behaves predominantly as a hard interacting entity. This also explains why all ΔE_{inter} values are positive, or in other words, why the hydroxide ion interacts better with the catalytic core than any of our proposed zinc ligands. Alternatively, the observed correlation could be explained by stating that the hardness decreases with increasing volume, and that the more voluminous fragments in our dataset fit worse into the active site due to steric hindrance. However, the absence of correlation in Figure 8 indicates that this is not the case.

Unfortunately, within the present dataset, the correlation observed in Figure 7 does not imply that η can be used as a measure for the total binding energy (Fig. 9). This is because ΔE_{tot} encompasses ΔE_{inter}, which decreases with η (Fig. 7), as well as ΔE_{prot}, which increases with η (Fig. 10). Consequently, the residual impact of the hardness on ΔE_{tot} is so small that it is over-

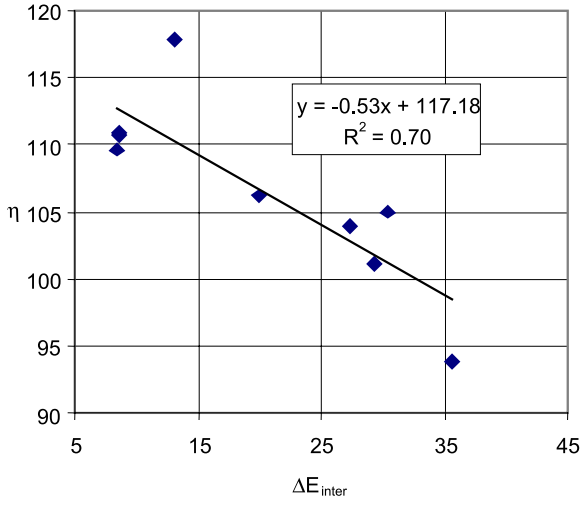

Figure 7. Correlation between the chemical hardness η (kcal mol^{-1}) and ΔE_{inter} (kcal mol^{-1}).

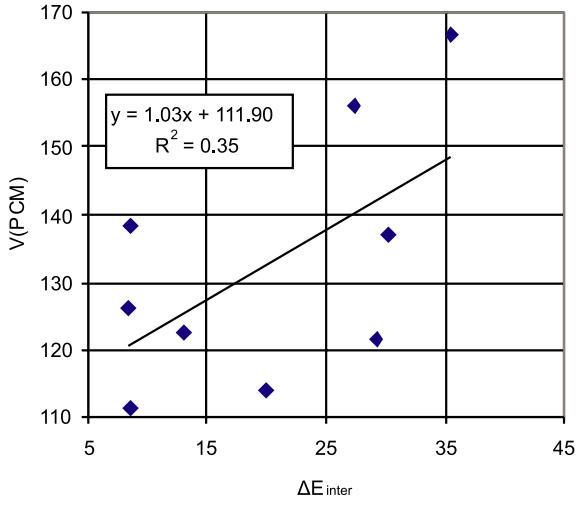

Figure 8. Correlation between the molecular volume as calculated by the PCM algorithm (Å^3) and ΔE_{inter} (kcal mol^{-1}).

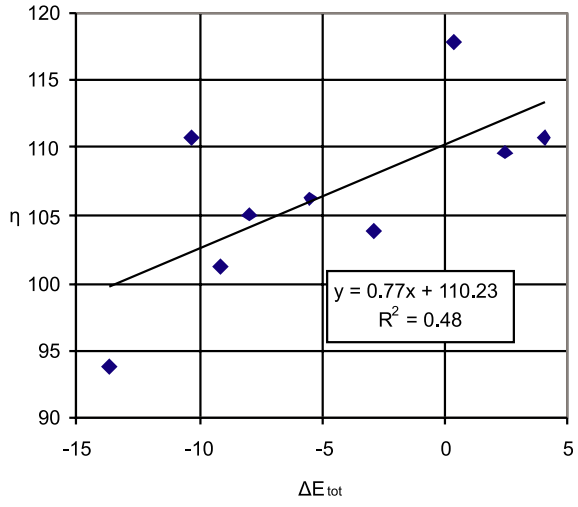

Figure 9. Correlation between the chemical hardness η (kcal mol^{-1}) and ΔE_{tot} (kcal mol^{-1}).

ruled by other contributions. More precisely, ΔE_{residu} also has a considerable impact on ΔE_{tot}. The most striking example of this is NMMTAA (**6**), which has both the worst ΔE_{inter} and the best ΔE_{tot}. This is the result of its low ΔE_{residu}, which may implicate a less favourable interaction with water, as well as its low ΔE_{prot}, which

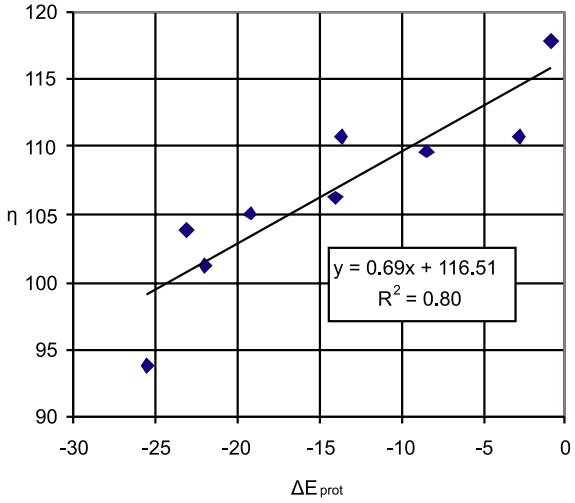

Figure 10. Correlation between the chemical hardness η (kcal mol^{-1}) and ΔE_{prot} (kcal mol^{-1}).

reflects its ease to donate a proton. As a general trend, ΔE_{residu} and ΔE_{prot} favour the sulfur-containing zinc-binding moieties in the ranking. At the other end of the range, HA (**11**) and NMHAA (**13**) are disfavoured by their low acidity. In fact, the ΔE_{prot} for HA (**11**) is so close to zero, that, taking into account the error on our calculations, it actually might not be deprotonated in the active site. Consequently, our results for this zinc-binding group might be inadequate for the purpose of validation and prediction.

NMNHU (**12**), on the other hand, is disfavoured by its high ΔE_{residu}, which is consistent with its presumed high polarity.

Finally, the contribution of ΔE_{conf} is always small. This reflects the high degree of rigidity in the active site model, and also indicates that our choice of constraining none of the active site hydrogen atoms might not be worth its computational cost. Added together, all these energetic contributions produce the ranking listed in Table 2.

4.3. Similarities between HDLP and hHDAC8

The significance of the present results depends on the premise that the catalytic core of HDLP is a good model for human HDACs in general and the class I HDACs in particular.[28,59,60] For one member of this class, HDAC8, a TSA-bound X-ray structure was recently published (PDB[45] entry code 1T64, resolution: 1.9 Å[21]). This structure can serve as a point of reference to test the validity of our model. Superposition of all 56 heavy atoms in this model with the corresponding atoms in HDAC8 (Fig. 11) yields an RMSD value of 0.41 Å. A closer examination learns that the measured RMSD is mainly the result of a repositioning of atoms that do not directly participate in binding (e.g., the phenyl ring of Tyr 297; for a detailed argumentation, see Ref. 41). Therefore, it is likely that the presented conclusions for HDLP also hold for HDAC8 and the other class I HDACs, albeit qualitatively.

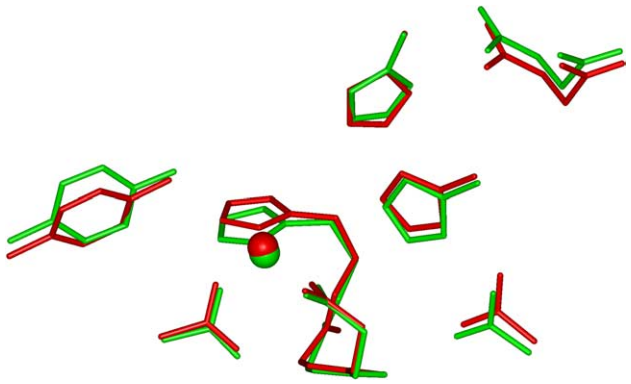

Figure 11. Superposition between the catalytic cores of HDLP (green) and hHDAC8 (red).

4.4. Experimental validation

Although the methodology of this study has a firm theoretical basis, an experimental validation is necessary to check the validity of the assumptions on which the active site model was based and to establish whether interaction energies of molecular fragments at 0 K have a practically useful predictive power. Unfortunately, the majority of the literature data is not useful for this purpose, because the present results cannot be correlated to assays performed on cell cultures. Therefore, only studies on free enzymes were considered. Still, these assays are often conducted on various mixtures of HDAC isoforms, which introduces a large uncertainty. Finally, results are almost always published as IC_{50} values, while K_i values are needed for a correct comparison. Because determination of the molar concentration of acetylated lysine side chains in a partially purified histone mixture is not a trivial task, this concentration is often not available, which rules out the option of directly converting IC_{50} values to K_i values with the Cheng–Prussoff equation:[61]

$$K_i = \frac{IC_{50}}{1 + S/K_m}.$$

However, starting from this equation, it can be shown that, within the same assay, ΔpIC_{50} values can be considered equal to ΔpK_i values, which makes extrapolation possible:

$$K_i = \frac{IC_{50}}{Cst_1} \iff -\log K_i = -\log IC_{50} + \log Cst_1$$
$$\Rightarrow \quad pK_i = pIC_{50} + Cst_2,$$

where Cst_1 and Cst_2 are constants that depend on the assay.

The known pK_i of TSA was taken as a starting point.[30] Then, an assay was performed in which both the pIC_{50} values of TSA and acetohydroxamate (AHA, **5**) were determined.[62] This makes it possible to use the above-mentioned equality of ΔpK_i and ΔpIC_{50}, so that

$$pK_i(\text{AHA}) = pK_i(\text{TSA}) + \Delta pIC_{50}(\text{AHA} - \text{TSA})$$
$$= 8.97 - 3.88 = 5.09 \text{ (see Table 3, row 2)}$$

The corresponding ΔG_{bind} of -7.2 kcal mol^{-1} could be regained by adding a $-T\Delta S$ term of +3.1 kcal mol^{-1} to a ΔH value approximated as equal to our ΔE_{tot} value. Since this $-T\Delta S$ value is within the range that can be expected for protein–ligand interactions,[63] it can be concluded that our calculations resulted in a realistic binding energy.

Likewise, the pK_i value of any zinc-binding group can be approximated by adding to pK_i(AHA) the ΔpIC$_{50}$ value between a hydroxamate-based HDAC inhibitor and an identical molecule with a different zinc-binding moiety, yielding the values in Table 3.

It should be noted that, since the cap group and the spacer part of the inhibitor molecule also contribute significantly to binding, ΔpIC$_{50}$ values from complete HDAC inhibitors are expected to be smaller than they would be if isolated molecular fragments were tested. The magnitude of this discrepancy will depend on the nature of the spacer and the cap group. For instance, the first data points for 1MP (**8**) and NMFHA (**9**) were determined on a cyclic tetrapeptide,[37,64,65] while the second data points for 1MP (**8**) and NMFHA (**9**), as well as the values for NMMAA (**10**) and NMNHU (**12**), were taken from studies of SAHA (**4**) derivatives.[38,66] Because of these important differences, not all of the experimental results may be comparable. Also, in the case of NMMAA (**10**), the calculated binding energy was shown to be unreliable due to steric interactions with a residue that was not included in our model (see Section 4.1), and thus is excluded from the regression analysis (Fig. 12). Given the many possible sources of error, this graph shows a good correlation, and at least suggests that the present method is suitable for the ranking of different zinc-binding moieties.

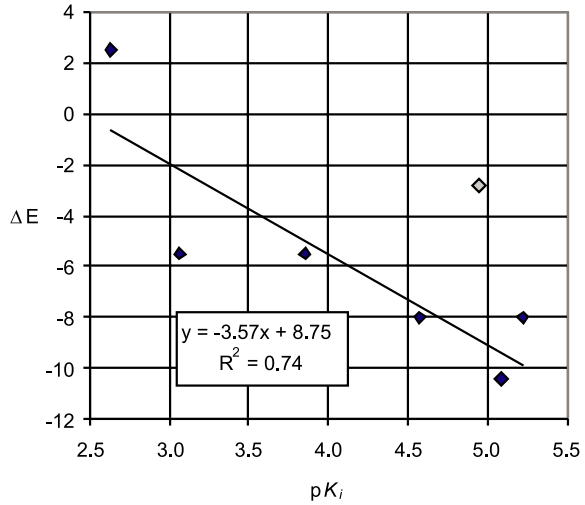

Figure 12. Correlation between theoretical ΔE (kcal mol^{-1}) and extrapolated experimental pK_i of HDAC-binding molecular fragments. The black line is the 'best fit' between all of the data points except NMMAA (**10**), which is shown in grey.

5. Conclusions

5.1. Design of new zinc ligands for incorporation in HDAC inhibitors

The current results show that designing new zinc-binding moieties for the purpose of incorporation in HDAC inhibitors is not a trivial task. As could be expected, bidentate chelators are shown to bind better than monodentate ligands. However, the conditions for having a bidentate binding mode like the hydroxamate (**5**) are very stringent. Indeed, the current results suggest that this goal cannot be accomplished if either centre A or D is a sulfur atom, or if centre C is an sp^3 carbon atom, ruling out many of the possibilities. Also, having a good hydrogen bond donor at centre C seems to be important for the binding affinity. Lastly, groups with a high chemical hardness interact best with the catalytic core, which is a drawback for strategies involving heavier atoms such as sulfur and phosphorus. However, it is interesting to note that increasing the acidity of the zinc-binding group may overcome some of these problems. Nevertheless, the acidity cannot be increased indefinitely, because the inhibitory potency of the zinc-binding group is expected the decrease exponentially when its pK_a is decreased below physiological pH, as argumented by Babine and Bender for the analogous case of the matrix metalloproteinases[67] and illustrated by the low binding affinities of carboxylate-based inhibitors.[11,24,34]

5.2. Empirical QSAR studies on HDAC inhibitors

The present breakdown of the binding energies of several zinc-binding groups into different contributions pro-

Table 3. Theoretical and extrapolated experimental affinities of HDAC-binding molecular fragments

Compound	ΔE (PCM)[a]	IC$_{50}$ (AHA)[b]/(nM)	IC$_{50}$ (nM)	ΔpIC$_{50}$	pK_i	References
TSA (**1**)					8.97	30
AHA (**5**)	−10.3	12[c]	91000	−3.88	5.09	62
1MP (**8**)	−8.0	0.38	1.25	−0.52	4.57	64,37
NMFHA (**9**)	−5.5	4.81	84	−1.24	3.85	65
1MP (**8**)	−8.0	280	210	+0.12	5.22	38
NMFHA (**9**)	−5.5	73	7800	−2.03	3.06	66
NMNHU (**12**)	+2.5	280	80000	−2.46	2.63	38
NMMAA (**10**)	−2.9	280	390	−0.14	4.95	38

[a] kcal mol^{-1}.
[b] This is the IC$_{50}$ of the corresponding hydroxamate.
[c] TSA.

vides a unique opportunity to increase the accuracy of QSAR models by providing a rational basis for selecting descriptors. As already noted above, the pK_a of the zinc-binding group plays a key role in this respect. From the energetic breakdown of NMNHU (**12**) versus AHA (**5**) and NMMAA (**10**) versus 1MP (**8**), it can be concluded that the energy of solvation also has an important influence of the binding energy, which suggests that the hydrophilicity, which is well known to affect pharmacokinetics, additionally could have a direct influence on pharmacodynamics. This finding supports the work of Sarkhel and Desiraju,[55] in which indications were found that the count of hydrogen donors and acceptors, which is integrated in 'Lipinsky's rule of five' as a measure for the hydrophilicity,[68] also may have implications in the context of intermolecular interactions.

However, the most interesting finding in this respect is the correlation between the chemical hardness and ΔE_{inter}. Chemical hardnesses of zinc-binding groups are easy and fast to calculate, and could provide a significant improvement for QSAR models, possibly even beyond HDAC inhibition research. However, if the ligand is a charged species like in the current study, it is shown that a QSAR model that incorporates the hardness should also include the pK_a in order to produce meaningful results. Providing that the active site geometry does not change too much upon ligand binding, the energetic breakdown in the current study could be completely mimicked by adding to this QSAR model a descriptor related to the hydrophilicity. Examples of these are the number of hydrogen bond donors and/or acceptors,[68] the hydrophobic component of the solvent-accessible surface, and log *P*, the latter two having been recently applied on a set of hydroxamate-based HDAC inhibitors.[69]

5.3. Replacement of the hydroxamate in existing HDAC inhibitors

Based on the geometry, the *N*-hydroxyformamide group (**9**) and the *N*′-hydroxyurea group (**12**) appear to be the most interesting possible replacements for the hydroxamate group (**5**) commonly found in HDAC inhibitors, because these groups display an identical binding mode, so that re-optimisation of the spacer is not required. However, the ΔE_{tot} values in Table 1 suggest that an *N*-hydroxyformamide (**9**) will not bind as good as a hydroxamate, probably because the H-bond with centre C is weaker. Also, substitution with the *N*′-hydroxyurea group (**12**) may have a large adverse effect on the binding affinity, because of the large energetic penalty on desolvation.

Since this study failed to identify any bidentate ligands containing sulfur, and since the presence of soft sulfur atoms negatively influences the ΔE_{inter}, the present results suggest that it is unlikely that sulfur-containing zinc-binding groups better than the hydroxamate will be found. However, as already suggested by Babine and Bender,[67] the ease of ionisation of the SH group compensates for its lower intrinsic affinity, and our study confirms that thiol-based zinc-binding moieties (**8**) are a viable alternative for the hydroxamate, although their binding affinities are still somewhat lower. The thiohydroxamate group (**7**) also might have a similar affinity as the hydroxamate, but this group may be less stable and synthetically challenging.[70] The results for the other groups considered in this study are inconclusive for the purpose of predicting binding affinities. Still, it is likely that they do not have the same bidentate-binding mode as the hydroxamate (**5**). For the sulfur-containing groups, this implies that the binding affinities will probably be close to that of the thiol-group, while the other groups are likely to display a lower binding affinity than the hydroxamate (**5**) and maybe even the *N*-hydroxyformamide (**9**). Still, some of these groups might be valid alternatives, for reasons of absorption and stability.

Acknowledgments

K. Vanommeslaeghe is a research assistant of the Fund for Scientific Research Flanders (Belgium) (F.W.O.-Vlaanderen). P. Geerlings also thanks the F.W.O.-Vlaanderen for continuous support of his research group. The authors are also grateful to G. Elaut, S. Coppens and V. Rogiers of the Department of Toxicology, Derma-Cosmetology and Pharmacognosy (FAFY) of the 'Vrije Universiteit Brussel' (Brussels, Belgium), for the binding data of TSA (**1**) and AHA (**5**).

References and notes

1. McLaughlin, F.; Finn, P.; La Thangue, N. B. *Drug Discov. Today* **2003**, *8*, 793–802.
2. Warrener, R.; Beamish, H.; Burgess, A.; Waterhouse, N. J.; Giles, N.; Fairlie, D.; Gabrielli, B. *FASEB J.* **2003**, *17*, 1550–1552.
3. Rombouts, K.; Niki, T.; Greenwel, P.; Vandermonde, A.; Wielant, A.; Hellemans, K.; De Bleser, P.; Yoshida, M.; Schuppan, D.; Rojkind, M.; Geerts, A. *Exp. Cell Res.* **2002**, *278*, 184–197.
4. Niki, T.; Rombouts, K.; De Bleser, P.; De Smet, K.; Rogiers, V.; Schuppan, D.; Yoshida, M.; Gabbiani, G.; Geerts, A. *Hepatology* **1999**, *29*, 858–867.
5. Papeleu, P.; Loyer, P.; Vanhaecke, T.; Elaut, G.; Geerts, A.; Guguen-Guillouzo, C.; Rogiers, V. *J. Hepatol.* **2003**, *39*, 374–382.
6. Mishra, N.; Brown, D. R.; Olorenshaw, I. M.; Kammer, G. M. *Proc. Natl. Acad. Sci. U.S.A.* **2001**, *98*, 2628–2633.
7. Leoni, F.; Zaliani, A.; Bertolini, G.; Porro, G.; Pagani, P.; Pozzi, P.; Dona, G.; Fossati, G.; Sozzani, S.; Azam, T.; Bufler, P.; Fantuzzi, G.; Goncharov, I.; Kim, S.-H.; Pomerantz, B. J.; Reznikov, L. L.; Siegmund, B.; Dinarello, C. A.; Mascagni, P. *Proc. Natl. Acad. Sci. U.S.A.* **2002**, *99*, 2995–3000.
8. McCampbell, A.; Taye, A. A.; Whitty, L.; Penney, E.; Steffan, J. S.; Fischbeck, K. H. *Proc. Natl. Acad. Sci. U.S.A.* **2001**, *98*, 15179–15184.
9. Steffan, J. S.; Joan, S.; Bodal, L.; Pallos, J.; Poelman, M.; McCampbell, A.; Apostol, B.; Kazantsev, A.; Schmidt, E.; Zhu, Y.-Z.; Greenwald, M.; Kurokawa, R.; Housman, D. E.; Jackson, G. R.; Marsh, J. L.; Thompson, L. M. *Nature* **2001**, *413*, 739–743.
10. Zhang, Y.; Li, N.; Caron, C.; Matthias, G.; Hess, D.; Khochbin, S.; Matthias, P. *EMBO J.* **2003**, *22*, 1168–1179.

11. Yoshida, M.; Kijima, M.; Akita, M.; Beppu, T. *J. Biol. Chem.* **1990**, *265*, 17174–17179.
12. Mori, K.; Koseki, K. *Tetrahedron* **1988**, *44*, 6013–6020.
13. Elaut, G.; Török, G.; Vinken, M.; Laus, G.; Papeleu, P.; Tourwé, D.; Rogiers, V. *Drug Metab. Dispos.* **2002**, *30*, 1320–1328.
14. Remiszewski, S. W.; Sambuchetti, L. C.; Atadja, P.; Bair, K. W.; Cornell, W. D.; Green, M. A.; Howell, K. L.; Jung, M.; Kwon, P.; Trogani, N.; Walker, H. *J. Med. Chem.* **2002**, *45*, 753–757.
15. Taunton, J.; Collins, J. L.; Schreiber, S. L. *J. Am. Chem. Soc.* **1996**, *118*, 10412–10422.
16. Meinke, P. T.; Liberator, P. *Curr. Med. Chem.* **2001**, *8*, 211–235.
17. Rosata, R. R.; Grant, S. *Expert. Opin. Investig. Drugs* **2004**, *13*, 21–38.
18. Saito, A.; Yamashita, T.; Mariko, Y.; Nosaka, Y.; Tsuchiya, K.; Ando, T.; Suzuki, T.; Tsuruo, T.; Nakanishi, O. *Proc. Natl. Acad. Sci. U.S.A.* **1999**, *96*, 4592–4597.
19. Richon, V. M.; Emiliani, S.; Verdin, E.; Webb, Y.; Breslow, R.; Rifkind, R. A.; Marks, P. A. *Proc. Natl. Acad. Sci. U.S.A.* **1998**, *95*, 3003–3007.
20. Finnin, M. S.; Donigian, J. R.; Cohen, A.; Richon, V. M.; Rifkind, R. A.; Marks, P. A.; Breslow, R.; Pavletich, N. P. *Nature* **1999**, *401*, 188–193.
21. Somoza, J. R.; Skene, R. J.; Katz, B. A.; Mol, C.; Ho, J. D.; Jennings, A. J.; Luong, C.; Arvai, A.; Buggy, J. J.; Chi, E.; Tang, J.; Sang, B.-C.; Verner, W.; Wynands, R.; Leahy, E. M.; Dougan, D. R.; Snell, G.; Navre, M.; Knuth, M. W.; Swanson, R. V.; Mcree, D. E.; Tari, L. W. *Structure* **2004**, *12*, 1325–1334.
22. Vannini, A.; Volpari, C.; Filocamo, G.; Casavola, E. C.; Brunetti, M.; Renzoni, D.; Chakravarty, P.; Paolini, C.; De Francesco, R.; Gallinari, P.; Steinkühler, C.; Di Marco, S. *Proc. Natl. Acad. Sci. U.S.A.* **2004**, *101*, 15064–15069.
23. Jung, M.; Hoffmann, K.; Brosch, G.; Loidl, P. *Bioorg. Med. Chem. Lett.* **1997**, *7*, 1655–1658.
24. Woo, S. H.; Frechette, S.; Khalil, E. A.; Boucain, G.; Vaisburg, A.; Bernstein, N.; Moradei, O.; Leit, S.; Allan, M.; Fournel, M.; Trachy-Bourget, M.-C.; Li, Z.; Besterman, J. M.; Delorme, D. *J. Med. Chem.* **2002**, *45*, 2877–2885.
25. Bouchain, G.; Leit, S.; Frechette, S.; Khalil, E. A.; Lavoie, R.; Moradei, O.; Woo, S. H.; Fournel, M.; Yan, P. T.; Kalita, A.; Trachy-Bourget, M.-C.; Beaulieu, C.; Li, Z.; Robert, M.-F.; MacLeod, A. R.; Besterman, J. M.; Delorme, D. *J. Med. Chem.* **2003**, *46*, 820–830.
26. Dai, Y.; Guo, Y.; Curtin, M. L.; Li, J.; Pease, L. J.; Guo, J.; Marcotte, P. A.; Glaser, K. B.; Davidsen, S. K.; Michaelides, M. R. *Bioorg. Med. Chem. Lett.* **2003**, *13*, 3817–3820.
27. Hu, E.; Dul, E.; Sung, C.-M.; Chen, Z.; Kirkpatrick, R.; Zhang, G.-F.; Johanson, K.; Liu, R.; Lago, A.; Hofmann, G.; Macarron, R. *J. Pharmacol. Exp. Ther.* **2003**, *307*, 720–728.
28. Park, J.-H.; Jung, Y.; Kim, T. Y.; Kim, S. G.; Jong, H.-S.; Lee, J. W.; Kim, D.-K.; Lee, J.-S.; Kim, N. K.; Kim, T.-Y.; Bang, Y.-J. *Clin. Cancer Res.* **2004**, *10*, 5271–5281.
29. Glaser, K. B.; Li, J.; Pease, L. J.; Staver, M. J.; Marcotte, P. A.; Guo, J.; Frey, R. R.; Garland, R. B.; Heyman, H. R.; Wada, C. K.; Vasudevan, A.; Michaelides, M. R.; Davidsen, S. K.; Curtin, M. L. *Biochem. Biophys. Res. Commun.* **2004**, *325*, 683–690.
30. Mai, A.; Massa, S.; Ragno, R.; Esposito, M.; Sbardella, G.; Nocca, G.; Scatena, R.; Jesacher, F.; Loidl, P.; Brosh, G. *J. Med. Chem.* **2002**, *45*, 1778–1784.
31. Mai, A.; Massa, S.; Cerbara, I.; Vanlente, S.; Ragno, R.; Bottoni, P.; Scatena, R.; Loidl, P.; Brosh, G. *J. Med. Chem.* **2004**, *47*, 1098–1109.
32. Lavoie, R.; Bouchain, G.; Frechette, S.; Woo, S. H.; Khalil, E. A.; Leit, S.; Fournel, M.; Yan, P. T.; Trachy-Bourget, M.-C.; Beaulieu, C.; Li, Z.; Besterman, J.; Delorme, D. *Bioorg. Med. Chem. Lett.* **2001**, *11*, 2847–2850.
33. Elaut, G.; Török, G.; Papeleu, P.; Vanhaecke, T.; Laus, G.; Tourwe, D.; Rogiers, V. *ATLA* **2004**, *32*, 105–112.
34. Colletti, S. L.; Myers, R. W.; Darkin-Rattray, S. J.; Gurnett, A. M.; Dulski, P. M.; Galuska, S.; Allocco, J. J.; Ayer, M. B.; Li, C.; Lim, J.; Crumley, T. M.; Cannova, C.; Schmatz, D. M.; Wyvratt, M. J.; Fisher, M. H.; Meinke, P. T. *Bioorg. Med. Chem. Lett.* **2001**, *11*, 107–111.
35. Wada, C. K.; Frey, R. R.; Ji, Z.; Curtin, M. L.; Garland, R. B.; Holms, J. H.; Li, J.; Pease, L. J.; Guo, J.; Glaser, K. B.; Marcotte, P. A.; Richardson, P. L.; Murphy, S. S.; Bouska, J. J.; Tapang, P.; Magoc, T. J.; Albert, D. H.; Davidsen, S. K.; Michaelides, M. R. *Bioorg. Med. Chem. Lett.* **2003**, *13*, 3331–3335.
36. Suzuki, T.; Nagano, Y.; Matsuura, A.; Kohara, A.; Ninomiya, S.; Kohda, K.; Miyata, N. *Bioorg. Med. Chem. Lett.* **2003**, *13*, 4321–4326.
37. Nishino, N.; Jose, B.; Okamura, S.; Ebisusaki, S.; Kato, T.; Sumida, Y.; Yoshida, M. *Org. Lett.* **2003**, *5*, 5079–5082.
38. Suzuki, T.; Nagano, Y.; Kouketsu, A.; Matsuura, A.; Maruyama, S.; Kurotaki, M.; Nakagawa, H.; Miyata, N. *J. Med. Chem.* **2005**, *48*, 1019–1032.
39. Vaisburg, A.; Bernstein, N.; Frechette, S.; Allan, M.; Abou-Khalil, E.; Leit, S.; Moradei, O.; Bouchain, G.; Wang, J.; Woo, S. H.; Fournel, M.; Yan, P. T.; Trachy-Bourget, M.-C.; Kalita, A.; Beaulieu, C.; Li, Z.; MacLeod, A. R.; Besterman, J. M.; Delorme, D. *Bioorg. Med. Chem. Lett.* **2004**, *14*, 283–287.
40. Vanommeslaeghe, K.; Van Alsenoy, C.; De Proft, F.; Martins, J. C.; Tourwé, D.; Geerlings, P. *Org. Biomol. Chem.* **2003**, *1*, 2951–2957.
41. Vanommeslaeghe, K.; De Proft, F.; Loverix, S.; Tourwé, D.; Geerlings, P. *Bioorg. Med. Chem.* **2005**, *13*, 3987–3992.
42. Ondetti, M. A.; Cushman, D. W. *CRC Crit. Rev. Biochem.* **1984**, *16*, 381–411.
43. Donini, O. A. T.; Kollman, P. A. *J. Med. Chem.* **2000**, *43*, 4180–4188.
44. Ferrara, P.; Gohlke, H.; Price, D. J.; Klebe, G.; Brooks, C. L., III *J. Med. Chem.* **2004**, *47*, 3032–3047.
45. Berman, H. M.; Westbrook, J.; Feng, Z.; Gilliland, G.; Bhat, T. N.; Weissig, H.; Shindyalov, I. N.; Bourne, P. E. *Nucleic Acids Res.* **2000**, *28*, 235–242.
46. Despite the fact that ESFF is developed for application on anorganic and organometallic molecules, it also is able to generate acceptable results, similar to CVFF, on organic compounds; see Martins, J. C.; Willem, R.; Biesemans, M. *J. Chem. Soc., Perkin Trans* **1999**, *2*, 1513–1520.
47. *Insight II version 98*, Accelrys (Formerly MSI).
48. Frisch, M. J.; Trucks, G. W.; Schlegel, H. B.; Scuseria, G. E.; Robb, M. A.; Cheeseman, J. R.; Montgomery, Jr., J. A.; Vreven, T.; Kudin, K. N.; Burant, J. C.; Millam, J. M.; Iyengar, S. S.; Tomasi, J.; Barone, V.; Mennucci, B.; Cossi, M.; Scalmani, G.; Rega, N.; Petersson, G. A.; Nakatsuji, H.; Hada, M.; Ehara, M.; Toyota, K.; Fukuda, R.; Hasegawa, J.; Ishida, M.; Nakajima, T.; Honda, Y.; Kitao, O.; Nakai, H.; Klene, M.; Li, X.; Knox, J. E.; Hratchian, H. P.; Cross, J. B.; Adamo, C.; Jaramillo, J.; Gomperts, R.; Stratmann, R. E.; Yazyev, O.; Austin, A. J.; Cammi, R.; Pomelli, C.; Ochterski, J. W.; Ayala, P. Y.; Morokuma, K.; Voth, G. A.; Salvador, P.; Dannenberg, J. J.; Zakrzewski, V. G.; Dapprich, S.; Daniels, A. D.; Strain, M. C.; Farkas, O.; Malick, D. K.; Rabuck, A. D.; Raghavachari, K.; Foresman, J. B.; Ortiz, J. V.; Cui, Q.; Baboul, A. G.; Clifford, S.; Cioslowski, J.; Stefanov, B. B.;

Liu, G.; Liashenko, A.; Piskorz, P.; Komaromi, I.; Martin, R. L.; Fox, D. J.; Keith, T.; Al-Laham, M. A.; Peng, C. Y.; Nanayakkara, A.; Challacombe, M.; Gill, P. M. W.; Johnson, B.; Chen, W.; Wong, M. W.; Gonzalez, C.; Pople, J. A. *Gaussian 03, Revision B.03*, Gaussian, Inc.: Wallingford, CT, 2003.

49. Boys, S. F.; Bernardi, F. *Mol. Phys.* **1970**, *19*, 553–566; Van Duijneveldt, F. B.; Van Duijneveldt; Van De Rijdt, J. G. C. M.; Van Lenthe, J. H. *Chem. Rev*. **1994**, *94*, 1873–1885.
50. Deppmeier, B. J.; Driessen, A. J.; Hehre, T. S.; Hehre, W. J.; Johnson, J. A.; Klunzinger, P. E.; Leonard, J. M.; Ohlinger, W. S.; Pham, I. N.; Pietro, W. J.; Yu, J.; *Spartan for Unix, v. 5.1*, Wavefunction: Irvine, CA, 1999.
51. Miertus, S.; Scrocco, E.; Tomasi, J. *Chem. Phys.* **1981**, *55*, 117–129.
52. Mennucci, B.; Cancès, E.; Tomasi, J. *J. Phys. Chem. B* **1997**, *101*, 10506–10517.
53. Cossi, M.; Scalmani, G.; Rega, N.; Barone, V. *J. Chem. Phys.* **2002**, *117*, 43–54.
54. For a comprehensive account on chemical hardness and related conceptual Density Functional Theory based reactivity descriptors, see Geerlings, P.; De Proft, F.; Langenaeker, W. *Chem. Rev.* **2003**, *103*, 1793–1873.
55. Sarkhel, S.; Desiraju, R. G. *Proteins* **2004**, *54*, 247–259.
56. Vargas, R.; Garza, J.; Dixon, D. A.; Hay, B. P. *J. Am. Chem. Soc.* **2000**, *122*, 4750–4755.
57. Scheiner, S.; Kar, T.; Gu, Y. *J. Biol. Chem.* **2001**, *276*, 9832–9837.
58. Hernick, M.; Fierke, C. A. *Arch. Biochem. Biophys.* **2005**, *433*, 71–84.
59. De Ruijter, A. J. M.; Van Gennip, A. H.; Caron, H. N.; Kemp, S.; Van Kuilenburg, A. B. P. *Biochem. J.* **2003**, *370*, 737–749.
60. Glaser, K. B.; Li, J.; Staver, M. J.; Wei, R.-Q.; Albert, D. H.; Davidsen, S. K. *Biochem. Biophys. Res. Commun.* **2003**, *310*, 529–536.
61. Cheng, Y.-C.; Prusoff, W. H. *Biochem. Pharmacol.* **1973**, *22*, 3099–3108.
62. Unpublished results by Elaut, G.; Rogiers, V. et al. The experimental details of the assay are described in an article titled ''Metabolic screening of hydroxamic acid-based histone deacetylase inhibitors in rat and human hepatocyte cultures'' (Elaut, G.; Laus, G.; Alexandre, E.; Vanhaecke, T.; Papeleu, P.; Richert, L.; Tourwé, D.; Rogiers, V. *J. Pharm. Exp. Ther.* **2005**, submitted). This assay is a variation on the one originally published by Kölle et al. (Kölle, D.; Brosch, G.; Lechner, T.; Lusser, A.; Loidl, P. *Methods* **1998**, *15*, 323–331).
63. Some relevant examples of calorimetric studies on comparable systems that yield similar $T\Delta S$ terms are: Aitken, S. M.; Turnbull, J. L.; Percival, M. D.; English, A. M. *Biochemistry* **2001**, *40*, 13980–13989; Parker, M. H.; Ortwine, D. F.; O'Brien, P. M.; Lunney, E. A.; Banotai, C. A.; Mueller, W. T.; McConnell, P.; Brouillette, C. G. *Bioorg. Med. Chem. Lett.* **2000**, *10*, 2427–2430.
64. Yoshida, M.; Furumai, R.; Nishiyama, M.; Komatsu, Y.; Nishino, N.; Horinouchi, S. *Cancer Chemother. Pharmacol.* **2001**, *48*, S20.
65. Nishino, N.; Yoshikawa, D.; Watanabe, L. A.; Kato, T.; Jose, B.; Komatsu, Y.; Sumida, Y.; Yoshida, M. *Bioorg. Med. Chem. Lett.* **2004**, *14*, 2427–2431.
66. Wu, T. Y. H.; Hassig, C.; Wu, Y.; Ding, S.; Schultz, P. G. *Bioorg. Med. Chem. Lett.* **2004**, *14*, 449–453.
67. Babine, R. E.; Bender, S. L. *Chem. Rev.* **1997**, *97*, 1359–1472.
68. Lipinski, C. A.; Lombardo, F.; Dominy, B. W.; Feeney, P. J. *Adv. Drug Deliv. Rev.* **1997**, *23*, 3–25.
69. Wang, D.-F.; Wiest, O.; Helquist, P.; Lan-Hargest, H.-Y.; Wiech, N. L. *Bioorg. Med. Chem. Lett.* **2004**, *14*, 707–711.
70. Chimiak, A.; Przychodzen, W.; Rachon, J. *Heteroatom Chem.* **2002**, *13*, 169–194.